https://doi.org/10.1007/s41230-024-3094-x

I-DCGAN and TOPSIS-IFP: A simulation generation model for radiographic flaw detection images in light alloy castings and an algorithm for quality evaluation of generated images

Ming-jun Hou[1], Hao Dong[1], *Xiao-yuan Ji[1], Wen-bing Zou[2], Xiang-sheng Xia[3], Meng Li[2], Ya-jun Yin[1], Bao-hui Li[4], Qiang Chen[3], and Jian-xin Zhou[1]

1. State Key Laboratory of Materials Processing and Die & Mould Technology, Huazhong University of Science and Technology, Wuhan 430074, China

2. Xinjiang Technology (Jiangsu) Co., Ltd., Nantong 226100, Jiangsu, China

3. Southwest Technique and Engineering Research Institute, Chongqing 400039, China

4. Shanghai Spaceflight Precision Machinery Institute, Shanghai 201600, China

Abstract: The intelligent detection technology driven by X-ray images and deep learning represents the forefront of advanced techniques and development trends in flaw detection and automated evaluation of light alloy castings. However, the efficacy of deep learning models hinges upon a substantial abundance of flaw samples. The existing research on X-ray image augmentation for flaw detection suffers from shortcomings such as poor diversity of flaw samples and low reliability of quality evaluation. To this end, a novel approach was put forward, which involves the creation of the Interpolation-Deep Convolutional Generative Adversarial Network (I-DCGAN) for flaw detection image generation and a comprehensive evaluation algorithm named TOPSIS-IFP. I-DCGAN enables the generation of high-resolution, diverse simulated images with multiple appearances, achieving an improvement in sample diversity and quality while maintaining a relatively lower computational complexity. TOPSIS-IFP facilitates multi-dimensional quality evaluation, including aspects such as diversity, authenticity, image distribution difference, and image distortion degree. The results indicate that the X-ray radiographic images of magnesium and aluminum alloy castings achieve optimal performance when trained up to the 800th and 600th epochs, respectively. The TOPSIS-IFP value reaches 78.7% and 73.8% similarity to the ideal solution, respectively. Compared to single index evaluation, the TOPSIS-IFP algorithm achieves higher-quality simulated images at the optimal training epoch. This approach successfully mitigates the issue of unreliable quality associated with single index evaluation. The image generation and comprehensive quality evaluation method developed in this paper provides a novel approach for image augmentation in flaw recognition, holding significant importance for enhancing the robustness of subsequent flaw recognition networks.

Keywords: light alloy casting; flaw detection image; generator; discriminator; comprehensive evaluation index

CLC numbers: TP391.9 **Document code:** A **Article ID:** 1672-6421(2024)03-239-09

1 Introduction

Magnesium, aluminum, and other light alloy castings have garnered widespread applications in crucial domains such as aviation, aerospace, and navigation due to their advantages, such as low density, high strength, and excellent corrosion resistance [1-2]. However, as the requirement for core equipment parts becomes higher and higher, the structure of light alloy castings has become more intricate, incorporating features such as wall thickness variations, multi-cross configurations,

***Xiao-yuan Ji**

Male, born in 1986, Associate Professor, doctoral supervisor. Research interests: Casting informatization, big data, workshop scheduling, algorithm, deep learning, defect identification, and laser additive.

E-mail: jixiaoyuan@hust.edu.cn

First author: Ming-jun Hou

E-mail: houmingjun21@163.com

Received: 2023-07-30; Accepted: 2023-10-31

multiple rings, curved surfaces, blind holes, and complex inner cavities, resulting in increased molding difficulty. At the same time, due to the influence of metal flow and cooling shrinkage, light alloy castings often have internal defects, such as shrinkage, dispersed shrinkage, and cracks [3]. These defects have a negative impact on the mechanical properties and reliability of castings. As a result, internal defect detection has become an indispensable process prior to the casting's departure from the factory.

The existing detection methods are mainly "X-ray flaw detection imaging + manual film evaluation". However, this method has the problems of missed detections, false detections, and inefficiency in flaw evaluation, which seriously threaten the performance and safety of aircraft and other equipment. Hence, the utilization of flaw detection technology propelled by X-ray images and deep learning becomes of paramount importance in achieving automated film evaluation [4-6] for detecting defects in light alloy castings. In recent years, with the rapid development of image processing [7], machine learning [8], deep learning [9], as well as the continuous improvement of digital image acquisition equipment and graphics processors [10], research on object detection and recognition driven by deep learning has been widely used in transportation [11], chips [12], and medicine [13]. However, due to the large scale span and various shapes of internal defects in castings, deep learning requires a large number of training samples to make the network performance robust [14-19]. What's more, in the actual application process, it is difficult to obtain a large number of flaw samples, which has also become a major obstacle restricting the engineering application of intelligent detection in the foundry industry.

In response to this problem, many scholars have carried out research on image augmentation and simulation generation. In 2018, Frid-Adar et al. [20] proposed to increase samples and improve the performance of image classification by synthesizing medical images through an adversarial network. In 2021, Mery [21] used GAN (Generative adversarial networks) to generate flaws, and projected them onto ray images to obtain defective image samples for defect detection and labeling research. In 2022, Mery et al. [22] used X-ray images to superimpose simulated targets based on Beer-Lambert law to generate training data. However, the existing research has not addressed the issues of poor diversity in flaw samples and low reliability in quality evaluation during the X-ray radiographic image augmentation for internal defects [23] in light alloy castings. Due to the high resolution of X-ray radiographic images of light alloy castings, directly using existing GAN networks makes it challenging to generate high-quality simulated images. Traditional mathematical transformations such as rotation are still used for image augmentation. The direct use of these images for training intelligent detection models has shown unsatisfactory results [24]. Additionally, when using GANs for simulation generation, there is a lack of comprehensive indexes for evaluating the quality of the generated images. Relying solely on the loss function or the FID (Fréchet Inception Distance) index does not fully explain the quality of the generated images, making it difficult to determine whether they are suitable for direct use in training intelligent detection models.

Therefore, in this study, the I-DCGAN (Interpolation-Deep Convolutional Generative Adversarial Networks) model and the TOPSIS-IFP (TOPSIS-IP/FID/PSNR) comprehensive evaluation algorithm were developed. The aim of this approach is to achieve the generation of high-resolution simulated images with diverse appearances and conducted multi-dimensional quality evaluations, including diversity, authenticity, image distribution differences, and image distortion degree, all while maintaining relatively low computational complexity. The framework is shown in Fig. 1.

2 Image simulation

Deep convolutional generative adversarial network [25] (DCGAN) is a classic generative adversarial network architecture for generating realistic images. DCGAN combines the ideas of deep convolutional neural network (CNN) and generative adversarial network (GAN), aiming to solve the problem of low image generation quality in traditional generative models. DCGAN is composed of two main components: Generator and discriminator. During the training process, DCGAN uses the augmented image as a real image input through confrontation training to fight against the fake image generated by the generator. This prompts the generator to generate more realistic and accurate flaw images, while the discriminator needs to learn to distinguish the difference between real images and generated images. Throughout the training process, not only does the generator's image generation proficiency undergoes continuous enhancement, but also the discriminator's ability to discriminate between real and generated images improves concomitantly.

There are a total of 39 flaw images of magnesium alloy and 880 flaw images of aluminum alloy. To minimize the computational complexity of the DCGAN network and enhance the performance of image generation, the difference algorithm was integrated into both the generator and discriminator, thereby formulating the I-DCGAN architecture. Additionally, data augmentation techniques were applied specifically to magnesium alloy images. Data augmentation is a method to generate more diverse and rich training samples by applying a series of transformations and processing to the original image.

The goal of data augmentation is to increase the quantity and quality of training data by introducing diversity and randomness, thereby improving the generalization ability and robustness of the model. By applying various transformation and warping operations to the original image, data augmentation can create new images with different perspectives, scales, light intensity conditions, and noise levels. For magnesium alloy images, following methods were used to help to improve the adaptability of the model under different angles and imaging parameters of X-ray flaw detection equipment: flipping (by flipping the image horizontally or vertically, the training set

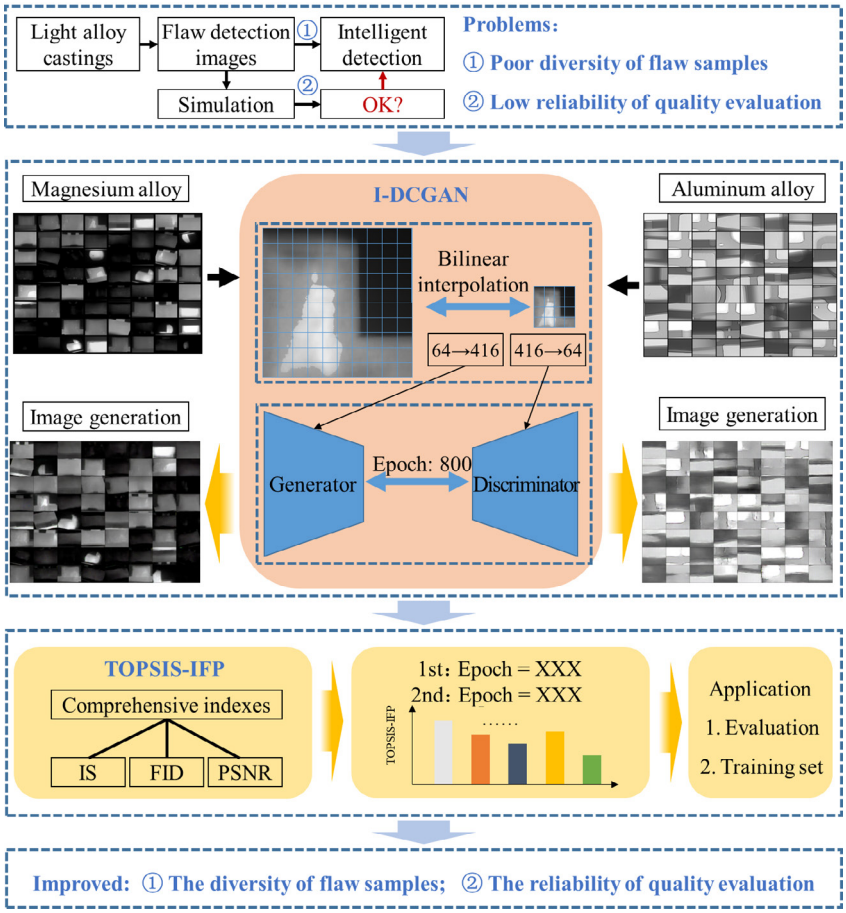

Fig. 1: I-DCGAN model and TOPSIS-IFP algorithm created in this study

can be extended and different angles of view can be simulated), cropping (by randomly cropping a part of the image and resizing it to a fixed size, different flaw sizes and positions can be simulated, providing position invariance to a certain extent), rotation (by rotating the image, the appearance of flaws at different angles can be simulated, which helps to improve the robustness of the model to rotation changes), scaling and translation (by adjusting the size and position of the image, flaws can be simulated under different distances and visual scales), brightness and contrast adjustment (by changing the brightness and contrast of the image, the appearance of flaws under different light intensity conditions can be simulated, which can increase the adaptability of the model to changes in light intensity), and noise increase (by introducing random noise to the image, the simulation of noise and interference in real-world scenarios can be achieved, thus bolstering the model's robustness and noise suppression capabilities). The advantage of employing augmented images as real training data for DCGAN lies in the introduction of a broader spectrum of image transformations and distortions. This approach enables the model to more effectively assimilate the distinctive characteristics and distribution of flaw images, as depicted in Fig. 2. By augmenting the original magnesium alloy images, applying augmentation once more to the augmented images, and utilizing a random selection method, a dataset of 9,984 magnesium alloy images is obtained.

The input, output, and structure of the constructed I-DCGAN network are shown in Fig. 3. The resolution of flaw detection images for magnesium and aluminum alloys is set at 416×416 pixels. Due to the limited memory capacity of commonly used computing platforms, especially PCs with a low-memory single graphics card, effectively accelerating deep learning models that require high-resolution images as input poses challenges. What's more, X-ray radiographic images of light alloy castings often have high resolutions, as seen in this study with a resolution of 416×416. If to directly construct a network structure without considering these high resolutions, not only the required number of network layers and computational complexity increase exponentially, but also the network structure struggles to effectively learn the training set features, especially when dealing with a limited amount of training data. To address this, the images were interpolated to substantially reduce computational complexity and network depth. This interpolation involves both upsampling and downsampling. Upsampling was used to increase the image resolution from 64×64 to 416×416, while downsampling to reduce the image resolution from 416×416 to 64×64. The generator takes a random sampling (channel =100, height or width=1) from the normal distribution space as its input. This input then passed through the network structure specified in Table 1, transforming it into a 3×64×64 image. Subsequently, the image was upsampled to a final size of 3×416×416. The

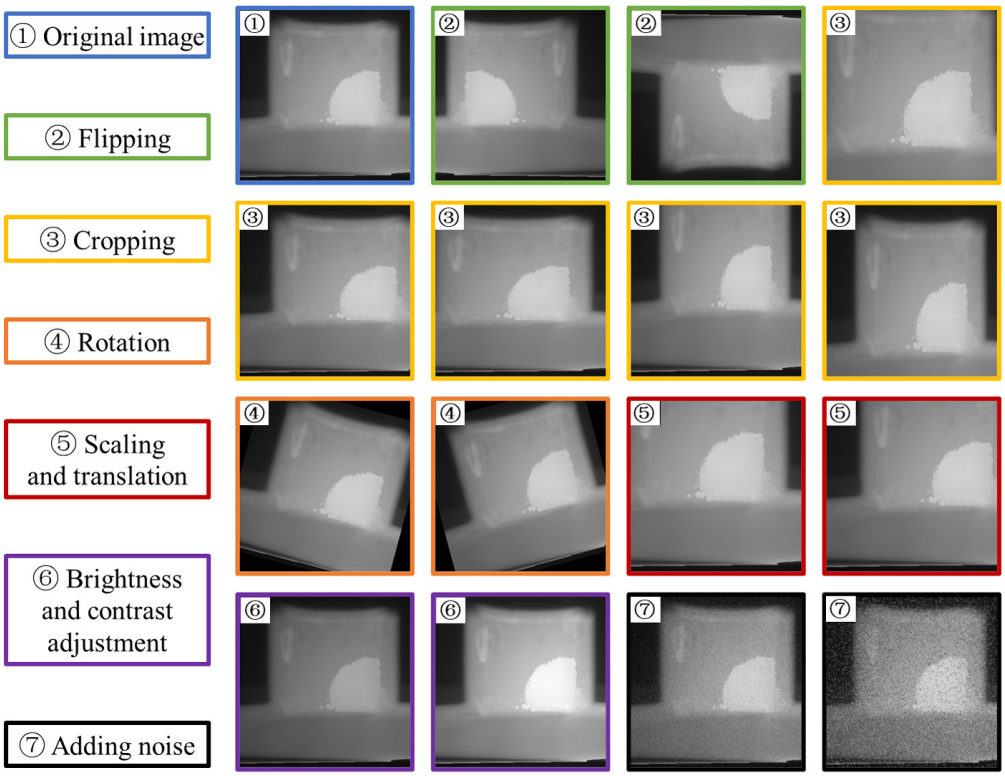

Fig. 2: Illustration of image augmentation

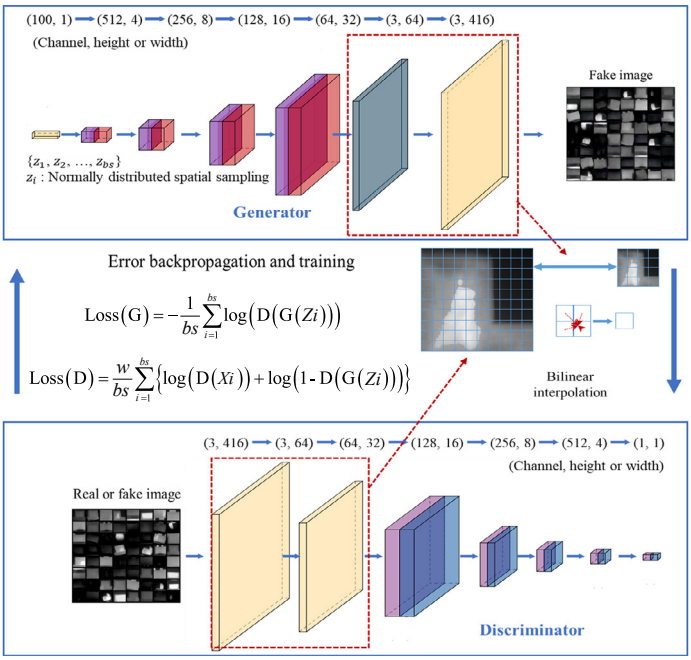

Fig. 3: Schematic diagram of I-DCGAN input, output, and network structure

input to the discriminator was a 3×416×416 image, which underwent downsampling to be converted into a 3×64×64 image. Subsequently, it traversed through the network structure depicted in Table 1, culminating in a final output size of 1. This output was utilized to discern the authenticity of the generated image. The hyperparameters were set as follows: the sampling space dimension of the generator input was 100, the loss function was binary cross-entropy loss, the optimization algorithm was Adam, the learning rate was 2e-4, the batch size was 128, and the number of epochs was 800.

The generator loss function is shown in Eq. (1), the discriminator loss function is shown in Eq. (2):

$$\mathrm{Loss}(\mathrm{G}) = -\frac{1}{bs}\sum_{i=1}^{bs}\log\left(\mathrm{D}\left(\mathrm{G}(Zi)\right)\right) \quad (1)$$

$$\mathrm{Loss}(\mathrm{D}) = \frac{w}{bs}\sum_{i=1}^{bs}\left\{\log\left(\mathrm{D}(Xi)\right) + \log\left(1-\mathrm{D}\left(\mathrm{G}(Zi)\right)\right)\right\} \quad (2)$$

where bs represents the batch size, w denotes the weight, typically set to 1. Zi is hidden space vectors obtained by sampling from a Gaussian distribution, G denotes the generator, and D stands for the discriminator. Xi is gray scale data representation of images obtained through sampling from the dataset.

The loss function and simulated images (composite simulated images generated by the generator at various training epochs, namely 1, 100, 200, ..., 800, with the existing parameter values) during the image training process of magnesium and aluminum alloys are shown in Fig. 4. Since I-DCGAN considers the overall image characteristics of the training set, it generates more diverse flaws than mathematical transformation augmentation methods such as rotation (traditional methods do not really enrich the flaw morphology). Regarding magnesium alloys, except for the models generated in the initial epoch, it is challenging to discern which epoch holds the highest image quality through human observation. Similarly, for aluminum alloys, aside from the initial three epochs, it is difficult to identify which epoch exhibits the highest image quality. Thus, it is suggested to create a comprehensive

Table 1: Network architecture of generator and discriminator (BN: batch normalization)

Network	Layer	Output size	Detail
Generator	Transposed Conv + BN + ReLu	512×4×4	Kernel size = (4, 4) Stride = (1, 1) Padding = (1, 1)
	Transposed Conv + BN + ReLu	256×8×8	Kernel size = (4, 4) Stride = (2, 2) Padding = (1, 1)
	Transposed Conv + BN + ReLu	128×16×16	Kernel size = (4, 4) Stride = (2, 2) Padding = (1, 1)
	Transposed Conv + BN + ReLu	64×32×32	Kernel size = (4, 4) Stride = (2, 2) Padding = (1, 1)
	Transposed Conv + Hard Tanh	3×64×64	Kernel size = (4, 4) Stride = (2, 2) Padding = (1, 1)
Discriminator	Conv + Leaky ReLu	64×32×32	Kernel size = (4, 4) Stride = (2, 2) Padding = (1, 1)
	Conv + BN + Leaky ReLu	128×16×16	Kernel size = (4, 4) Stride = (2, 2) Padding = (1, 1)
	Conv + BN + Leaky ReLu	256×8×8	Kernel size = (4, 4) Stride = (2, 2) Padding = (1, 1)
	Conv + BN + Leaky ReLu	512×4×4	Kernel size = (4, 4) Stride = (2, 2) Padding = (1, 1)
	Conv + Sigmoid	1	Kernel size = (4, 4) Stride = (2, 2) Padding = (0, 0)

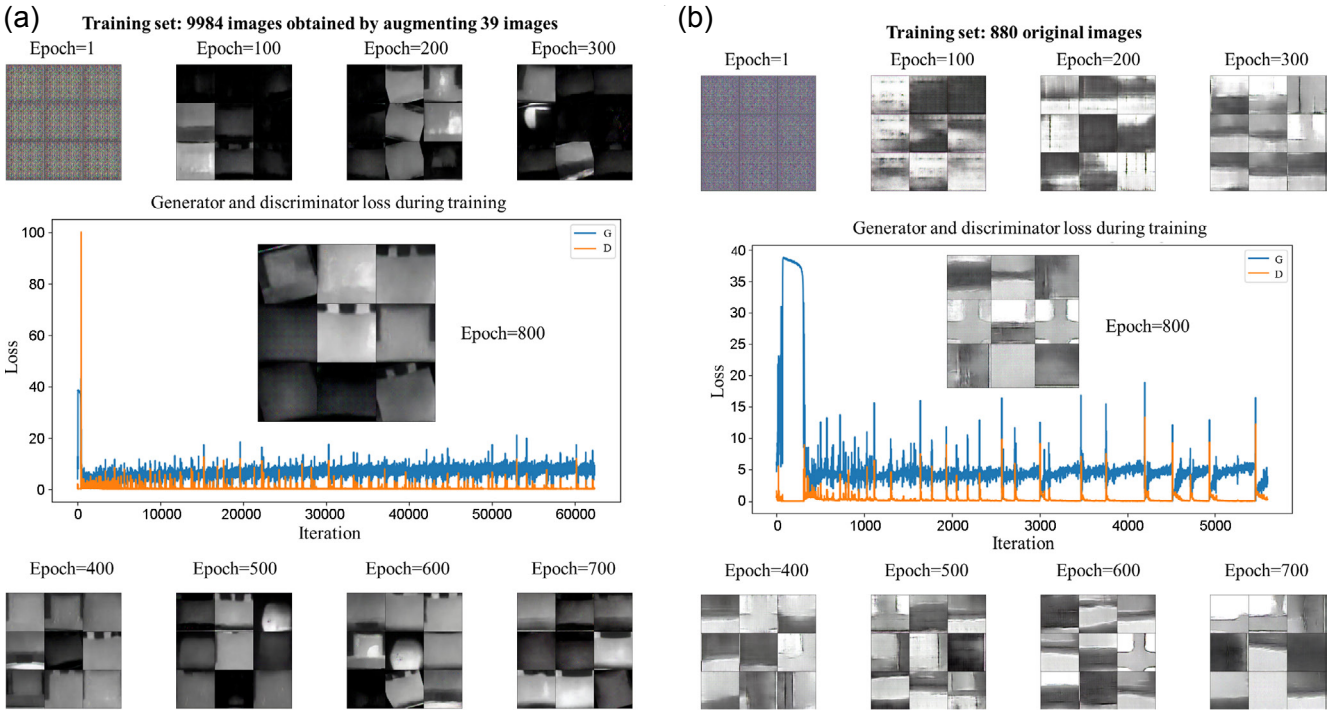

Fig. 4: Schematic diagram of image training loss function and effect of generated image: (a) magnesium alloy; (b) aluminum alloy

evaluation index for simulated flaw detection images of light alloy castings, in order to choose the best generative model from the 800 training epochs.

3 Quality evaluation

In order to quantitatively evaluate the quality of generated flaw detection images, a comprehensive evaluation algorithm for simulated images was proposed, combined with inception score (IS), Fréchet inception distance (FID), and peak signal-to-noise ratio (PSNR) to assess simulated images from various dimensions, including diversity, authenticity, image distribution difference, and image distortion degree.

Inception score aims to measure the diversity and realism of generated images. Diversity means that GAN can generate images of different categories and styles; trueness means that the generated images and real images have a similar distribution in the feature space. The IS calculation method includes calculating the class probability distribution of each generated image and calculating the KL (Kullback-Leibler) divergence. Firstly, employ the pre-trained inception model to perform forward propagation on each generated image, obtaining the output of each image on the Inception model. Subsequently, for each image in the generated image collection, calculate the KL divergence between its class probability distribution and the average class probability distribution of the entire generated image collection. Finally, take the average as the final IS. Generally, a higher IS indicates that the generated images have better diversity and realism.

FID aims to measure the difference between the distribution of generated image and the real image. It uses the statistical information of the feature vectors extracted by the inception model to calculate the distance between distributions. FID takes into account the diversity and quality of generated images, where a lower FID value indicates a smaller difference between the distribution of generated images and real images. The FID calculation steps are as follows: firstly, use the pre-trained Inception model to perform forward propagation on the real image and the generated image, and extract the feature vector of each image; secondly, calculate the mean value and covariance matrix of the feature vector; finally, utilize the mean vector and covariance matrix of the real image feature vector as the reference distribution, and generate the mean vector and covariance matrix of the image feature vector as the test distribution. Then, calculate the Fréchet distance between the reference distribution and the test distribution to quantify the disparity between the two distributions.

PSNR is used to measure the degree of distortion of the image, that is, the difference between the processed or compressed image and the original one. The higher the PSNR value, the lower the distortion of the image and the better the quality. The calculation method is as follows: firstly, the original image and the processed one are used as a matrix; secondly, the difference between them is calculated pixel by pixel, and the square is calculated; thirdly, the results of all the squares are added and divided by the number of pixels of the image to obtain the mean square error; finally, the peak signal-to-noise ratio is calculated.

In order to integrate multiple evaluation indexes and assess the quality of generated flaw detection images effectively, TOPSIS-IFP comprehensive evaluation algorithm using the TOPSIS (Technique for Order of Preference by Similarity to Ideal Solution) method [26] was proposed. Comprehensive consideration of the weights and differences among indexes provides more accurate evaluation results. The followings are the detailed calculation steps of TOPSIS-IFP:

Firstly, each index was normalized to a range between 0 and 1. For IS and PSNR, the index value is subtracted from the minimum value and divided by the difference between the maximum value and the minimum value when normalizing, as shown in Eq. (3):

$$NS = (S\text{-}MINS) / MAXS\text{-}MINS \tag{3}$$

where NS is the standardized score, S is the original score, $MINS$ is the minimum score, and $MAXS$ is the maximum score.

For indexes that bigger is better (such as IS and PSNR), they are directly processed according to Eq. (3). For FID, it is processed in a reciprocal manner, as shown in Eq. (4):

$$NS = (IS\text{-}MINS) / MAXIS\text{-}MINIS \tag{4}$$

where $MAXIS$ represents the maximum value after taking the reciprocal of the index, and $MINIS$ represents the minimum value after taking the reciprocal of the index.

Secondly, each index is assigned a weight, and a decision matrix is constructed to reflect its importance in the quality evaluation of generated flaw detection images. Since the flaw detection image is different from the natural one, the evaluation based on IS will show a large value when the epoch is small. At this juncture, the quality of the casting appears significantly blurred, making it challenging to generate a recognizable flaw detection image. PSNR measures the peak signal-to-noise ratio between the generated image and the original one, and the evaluation is relatively one-sided. Therefore, the weights of these two indexes are set to be small. In this case, the weights of IS, FID, and PSNR are set to 0.2, 0.6, and 0.2, respectively. In the constructed decision matrix, each row represents a solution (the generated flaw detection image), each column represents an evaluation index, and the standardized index values are filled into the decision matrix.

Thirdly, determine the ideal solution and the negative ideal solution, which is also a key step in the TOPSIS method. An ideal solution means each index takes the maximum value, while a negative ideal solution is on the contrary. By calculating the Euclidean distance, the distance between the positive ideal solution and negative one can be obtained. Next, calculate the proximity of each solution by comparing the distance between the negative ideal solution and the ideal solution to the distance between the practical solution and the ideal solution.

Finally, the solutions are ranked according to their closeness (TOPSIS-IFP value), which is used to characterize the quality of the comprehensive evaluation results, as shown in Fig. 5.

Based on the flaw detection images of magnesium and aluminum alloys generated in the previous steps, the quality of the simulated images is comprehensively evaluated for the training epochs at 100, 200, 300, 400, 500, 600, 700, and 800. The above generation models were named as Mg-E100, Mg-E200, Mg-E300, Mg-E400, Mg-E500, Mg-E600, Mg-E700, Mg-E800, Al-E100, Al-E200, Al-E300, Al-E400, Al-E500, Al-E600, Al-E700, Al -E800. Each model generates 640 simulated images, the evaluation batch size is 64 (64 images are evaluated as a group), and each model obtains 10 values for each index. After discarding the maximum and minimum values and calculating the averages, the values of the three indexes for each model are presented in Table 2. The evaluation score trend chart can be viewed in Fig. 6(a).

The weights of IS, FID, and PSNR are set to 0.2, 0.6, and 0.2, respectively. Comprehensive scores are calculated according to the TOPSIS-IFP, as shown in Table 2 and Fig. 6(b). For the magnesium alloy model, the optimal order is E800, E600, E400, E700, E500, E200, E300, E100; for the aluminum alloy model, the optimal order is E600, E800, E700, E100, E500, E300, E400, E200. Figure 7 illustrates the comparison of generated images arranged in the ranking order of comprehensive indexes and the optimal images corresponding to different indexes.

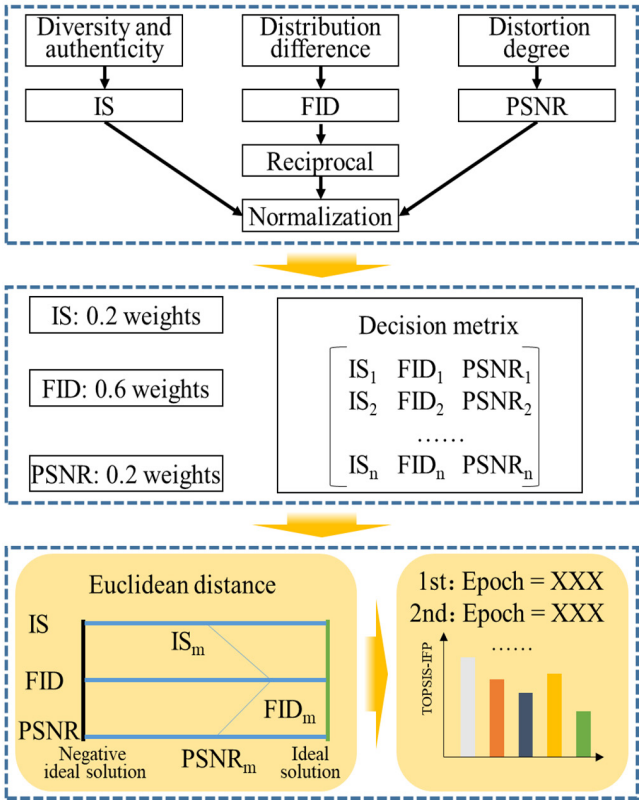

Fig. 5: TOPSIS-IFP scheme diagram

Table 2: Single index and TOPSIS-IFP evaluation form

Alloy	Index	E100	E200	E300	E400	E500	E600	E700	E800
Mg	IS	3.98	3.87	2.87	2.90	3.18	2.72	2.70	2.92
	FID	883.74	683.90	693.50	617.38	630.02	591.40	597.42	570.40
	PSNR	15.32	15.90	15.37	15.66	15.33	15.61	15.53	15.80
	TOPSIS-IFP	0.240	0.598	0.435	0.681	0.612	0.706	0.679	0.787
Al	IS	9.28	5.19	5.42	5.49	6.23	4.53	3.55	4.04
	FID	1,652.11	1,610.48	1,588.71	1,587.00	1,586.97	1,328.52	1,290.41	1,333.24
	PSNR	15.98	15.61	15.86	15.75	16.16	16.20	15.98	16.44
	TOPSIS-IFP	0.264	0.118	0.183	0.173	0.259	0.738	0.730	0.726

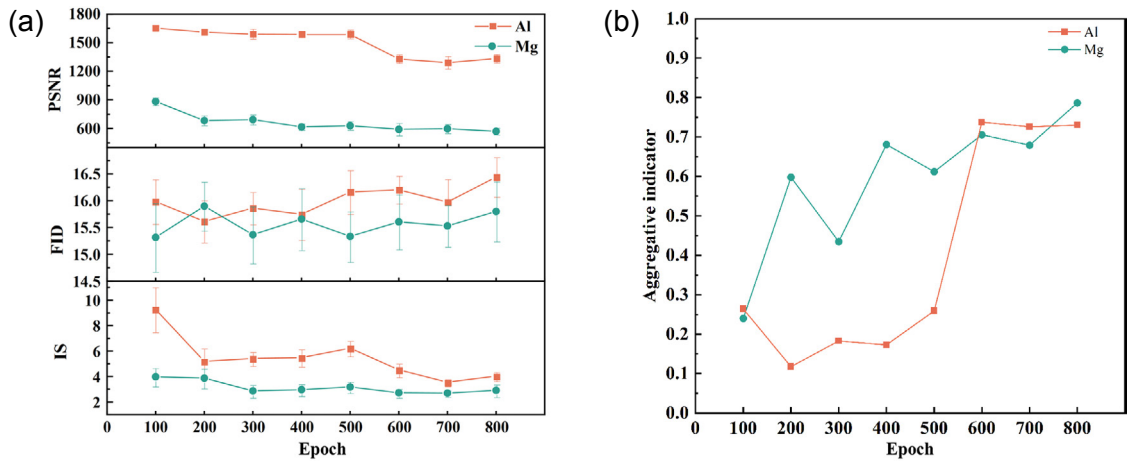

Fig. 6: Single index and TOPSIS-IFP evaluation chart: (a) single index; (b) TOPSIS-IFP index

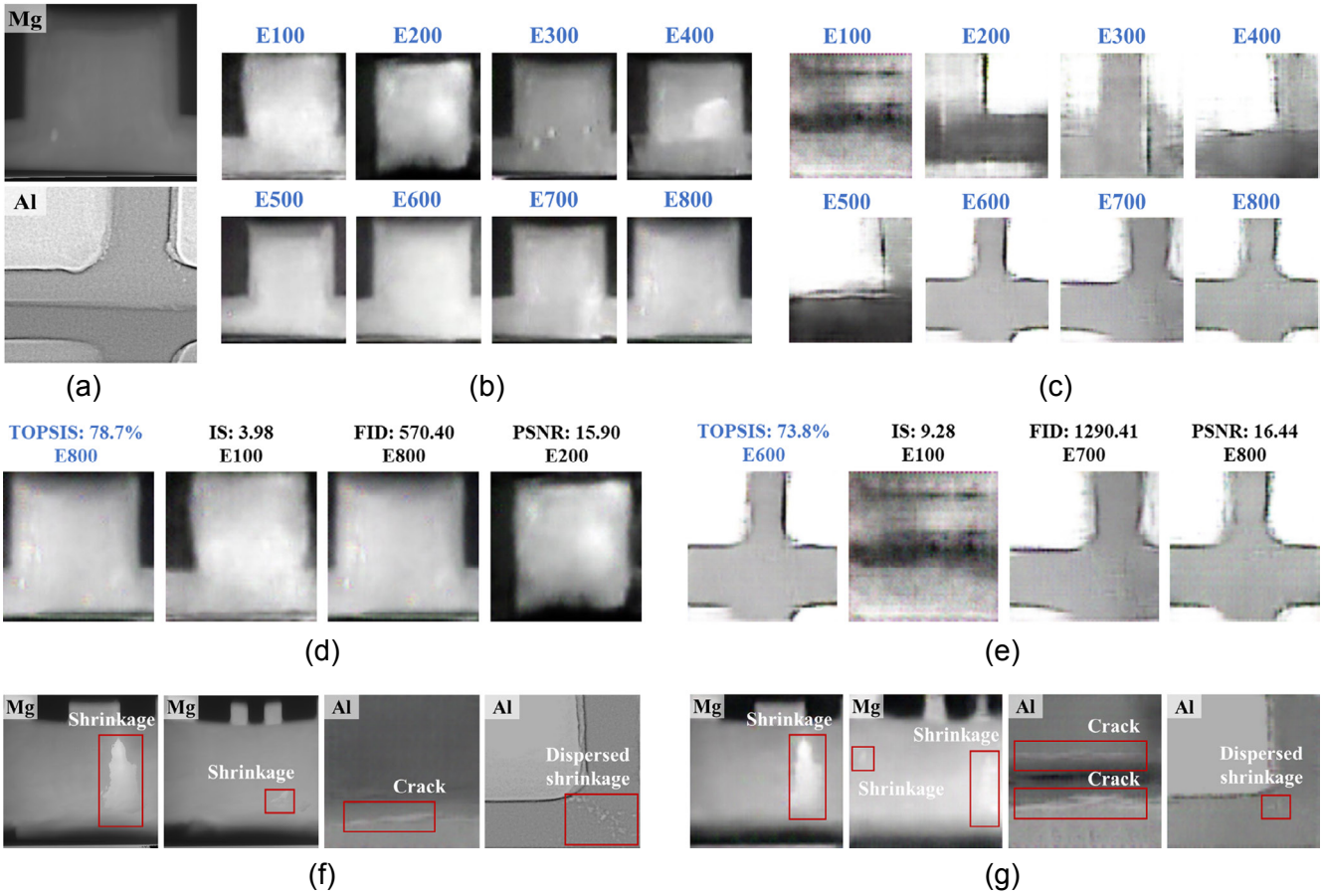

Fig. 7: Comprehensive ranking of generated images and comparison of optimal image in different indexes: (a) original image; (b) magnesium alloy generated images; (c) aluminum alloys generated images; (d) optimal image comparison of magnesium alloy with different indexes; (e) optimal image comparison of aluminum alloy with different indexes; (f) real defect images; (g) TOPSIS-IFP optimum simulated defect images

For the X-ray radiographic images of magnesium and aluminum alloys, training the models up to the 800th and 600th epochs respectively, the TOPSIS reaches its optimal value, with a similarity to the ideal solution of 78.7% and 73.8%, respectively. According to Table 2, the X-ray radiographic images of magnesium alloy in E600 and E800, as well as aluminum alloy in E600, E700, and E800, exhibit a high degree of similarity (over 70%) to the ideal solution. Compared to other epochs, these epochs demonstrate higher-quality generated images, as illustrated in Figs. 7(b and c). The TOPSIS-IFP algorithm can effectively select higher-quality simulated images based on their similarity to the ideal solution, which is an advantage that single index evaluation lacks.

As shown in Figs. 7(d and e), the single index optimal epochs for magnesium alloy are E100, E800, and E200 for IS, FID, and PSNR, respectively. For aluminum alloy, the single index optimal epochs are E100, E700, and E800 for IS, FID, and PSNR, respectively. The FID index identifies E800 as the optimal for evaluating simulated magnesium alloy images, which aligns with the TOPSIS-IFP result. However, for aluminum alloy simulated images, the optimal epoch according to FID is E700, which is not reliable. The generated images from E700 exhibit noticeably lower edge clarity compared to the TOPSIS-IFP's optimal epoch, E600. In the evaluation of simulated aluminum alloy images, the PSNR identifies E800 as the optimal, while for magnesium alloy, it selects E200 as the best. However, the visual quality of the generated images is quite poor, as depicted in Figs. 7(f and g), which showing the real defect instances and simulated defect instances.

The above results imply that the TOPSIS-IFP evaluation algorithm performs better than the limited single index evaluation, effectively mitigating the problem of unreliable quality.

4 Conclusions

(1) The I-DCGAN network structure is constructed, considering the high-resolution feature of X-ray radiographic images of light alloy castings. To address this characteristic, an interpolation algorithm is incorporated into the network structure. This allows for the generation of high-resolution simulated images with diverse appearances, all while maintaining a relatively lower computational complexity. Consequently, it significantly improves both the diversity and quality of the generated samples. Furthermore, this approach effectively addresses the issue of poor diversity in flaw samples that has been present in mathematical transformation augmentation methods such as rotation.

(2) A TOPSIS-IFP comprehensive evaluation algorithm is

proposed, which realizes multi-dimensional quality evaluation such as diversity, authenticity, image distribution difference, and image distortion degree. For the X-ray radiographic images of magnesium and aluminum alloy castings, training the models up to the 800th and 600th epochs respectively, the TOPSIS-IFP value reaches its optimal value, with a similarity to the ideal solution of 78.7% and 73.8% respectively. Compared to single index evaluation, the TOPSIS-IFP algorithm achieves higher-quality simulated images at the optimal training epoch, effectively mitigating the problem of unreliable quality.

The image generation and comprehensive quality evaluation method developed in this study provides a new approach for image augmentation in flaw recognition, holding significant importance in enhancing the robustness of subsequent flaw recognition networks.

Acknowledgments

This research was funded by the National Key R&D Program of China (2020YFB1710100), and the National Natural Science Foundation of China (Nos. 52275337, 52090042, 51905188).

Conflict of interest

Jian-xin Zhou is an EBM of *CHINA FOUNDRY*. He was not involved in the peer-review or handling of the manuscript. The authors have no other competing interests to disclose.

References

[1] Liu B, Yang J, Zhang X Y, et al. Development and application of magnesium alloy parts for automotive OEMs: A review. Journal of Magnesium and Alloys, 2023, 11(1): 15–47.
[2] Garg P, Jamwal A, Kumar D, et al. Advance research progresses in aluminium matrix composites: Manufacturing & applications. Journal of Materials Research and Technology, 2019, 8(5): 4924–4939.
[3] Feng S K, Liotti E, Grant P S. X-ray imaging of alloy solidification: Crystal formation, growth, instability and defects. Materials, 2022, 15(4): 1319.
[4] Ji X Y, Yan Q Y, Huang D, et al. Filtered selective search and evenly distributed convolutional neural networks for casting defects recognition. Journal of Materials Processing Technology, 2021, 292(2): 117064.
[5] Wu B, Zhou J X, Ji X Y, et al. An ameliorated teaching-learning-based optimization algorithm based study of image segmentation for multilevel thresholding using Kapur's entropy and Otsu's between class variance. Information Sciences, 2020, 533(9): 72–107.
[6] Wu B, Zhou J X, Yang H Q, et al. An ameliorated deep dense convolutional neural network for accurate recognition of casting defects. Knowledge-Based Systems, 2021, 226(8): 107096.
[7] Fu W L, Jiang X H, Li B L, et al. Rolling bearing fault diagnosis based on 2D time-frequency images and data augmentation technique. Measurement Science and Technology, 2023, 34(4): 045005.
[8] Wei H Y, Wu C T, Hu W, et al. LS-DYNA machine learning-based multiscale method for nonlinear modeling of short fiber-reinforced composites. Journal of Engineering Mechanics, 2023, 149(3): 04023003.
[9] Lian G H, Sun Q H, Liu X M, et al. Automatic recognition and intelligent analysis of central shrinkage defects of continuous casting billets based on deep learning. Journal of Iron and Steel Research International, 2023, 30: 937–948.
[10] Goodfellow I, Bengio Y, Courville A. Deep learning. The MIT Press, 2016.
[11] Kuutti S, Bowden R, Jin Y C, et al. A survey of deep learning applications to autonomous vehicle control. IEEE Transactions on Intelligent Transportation Systems, 2021, 22(2): 712–733.
[12] Irhoseini A, Goldie A, Yazgan M, et al. A graph placement methodology for fast chip design. Nature, 2021, 594(7862): 207–212.
[13] Richard J C, Ming Y L, Wang J W, et al. Pathomic fusion: An integrated framework for fusing histopathology and genomic features for cancer diagnosis and prognosis. IEEE Transactions on Medical Imaging, 2020, 41(4): 757–770.
[14] Wang L, Dong X, Guo S. Sand-bed defect recognition for 3D sand printing based on deep residual network. China Foundry, 2021, 18(4): 344–350.
[15] Han Y, Li X J, Song K C, et al. Adaptive depth and receptive field selection network for defect semantic segmentation on castings X-rays. NDT & E International, 2020, 116(6): 102345.
[16] Yang K, Sun Z Y, Wang A H, et al. Deep hashing network for material defect image classification. IET Computer Vision, 2018, 12(8): 1112–1120.
[17] Jing R, Rui R, Mark G, et al. Defect detection from X-Ray images using a three-stage deep learning algorithm. In: Proc. 2019 IEEE Canadian Conference of Electrical and Computer Engineering (CCECE). IEEE, 2019: 1–4.
[18] Hu C F, Wang Y X, Chen K, et al. A CNN model based on spatial attention modules for casting type classification on pseudo-color digital radiography images. In: Proc. 2019 Chinese Automation Congress (CAC2019), 2019: 4585–4589.
[19] Hu C F, Wang Y X. An efficient convolutional neural network model based on object-level attention mechanism for casting defect detection on radiography images. IEEE Transactions on Industrial Electronics, 2020, 67(12): 10922–10930.
[20] Frid-Adar M, Diamant I, Klang E, et al. GAN-based synthetic medical image augmentation for increased CNN performance in liver lesion classification. Neurocomputing, 2018, 321: 321–331.
[21] Mery D. Aluminum casting inspection using deep object detection methods and simulated ellipsoidal defects. Machine Vision and Applications, 2021, 32(3): 1–16.
[22] Mery D, Kaminetzky A, Golborne L, et al. Target detection by target simulation in X-ray testing. Journal of Nondestructive Evaluation, 2022, 41(1): 21.
[23] Hou Y, Wu M, Huang F, et al. Defect band formation in high pressure die casting AE44 magnesium alloy. China Foundry, 2022, 19(3): 201–210.
[24] Bahmei B, Birmingham E, Arzanpour S. CNN-RNN and data augmentation using deep convolutional generative adversarial network for environmental sound classification. IEEE Signal Processing Letters, 2022, 29: 682–686.
[25] Radford A, Metz L, Chintala S. Unsupervised representation learning with deep convolutional generative adversarial networks. arXiv e-prints, 2015: 1511.06434.
[26] Wang Y M, Liu P D, Yao Y Y. BMW-TOPSIS: A generalized TOPSIS model based on three-way decision. Information Sciences, 2022, 607: 799–818.